Electrochemical oxidation of Pt(111) beyond the place-exchange model

Jacobse, L.; Vonk, V.; McCrum I.T.; Seitz, C.; Koper, M.T.M.; Rost, M.J.; Stierle, A.

Electrochimica Acta 407 (2022) 139881

Contents lists available at ScienceDirect

Electrochimica Acta

journal homepage: www.elsevier.com/locate/electacta

Electrochemical oxidation of Pt(111) beyond the place-exchange model

Leon Jacobse[a,*], Vedran Vonk[a], Ian T. McCrum[b], Christoph Seitz[a], Marc T.M. Koper[d], Marcel J. Rost[c], Andreas Stierle[a]

[a] Centre for X-ray and Nano Science CXNS, Deutsches Elektronen-Synchrotron DESY, Notkestrasse 85, D-22607 Hamburg, Germany
[b] Department of Chemical and Biomolecular Engineering, Clarkson University, Potsdam, New York 13699, United States
[c] Huygens-Kamerlingh Onnes Laboratory, Leiden University, PO Box 9504, 2300 RA Leiden, the Netherlands
[d] Leiden Institute of Chemistry, Leiden University, PO Box 9502, 2300 RA Leiden, the Netherlands

ARTICLE INFO

Article history:
Received 24 July 2021
Revised 7 January 2022
Accepted 8 January 2022
Available online 10 January 2022

Keywords:
Pt(111)
Pt oxidation
Surface X-ray diffraction
Place-Exchange
Surface roughening

ABSTRACT

Oxide formation plays an important role in the degradation of Pt electrocatalysts. However, the exact oxide structure and reaction mechanism are not fully understood. Here, we used in situ surface X-ray diffraction experiments to resolve the oxide formation at a Pt(111) model electrode at potentials near the onset of the oxygen evolution reaction. Fast experiments are possible by using X-ray photons with a high kinetic energy in combination with a large 2D detector. By employing very low potential sweep rates we obtain a more ordered oxidized surface compared to literature data from potential step experiments. This demonstrates that the oxidation process is strongly governed by the reaction kinetics. The increased surface order enables us to disentangle two subsequent oxidation process; initially the place-exchange process, followed by the formation of a partially disordered oxide in which still 50% of the surface atoms reside on sites commensurate to the Pt(111) surface. The reduction experiments indicate that the place-exchange process is structurally reversible, whereas the disordered oxide causes the surface roughening observed during potential cycling. Despite the increased surface order, oxide superstructures are not observed. These results provide important insights in the oxidation and degradation process of Pt(111), which are valuable for the design of improved electrocatalysts and they rationalize operating procedures.

1. Introduction

Platinum electrodes are extensively studied because of their high reactivity for reactions involved in sustainable energy technologies, such as hydrogen oxidation and oxygen reduction in fuel cells. Their widespread technological application, however, is hindered by degradation of the expensive electrodes. Many of the degradation phenomena, such as Pt dissolution, surface restructuring, or delamination, occur largely upon the application of oxidizing potentials [1,2]. The effect of the degradation on the electrode surface structure, can be assessed in potential cycling experiments, where oxidizing and reducing potentials are applied alternatingly. Studies employing such procedures using model electrodes have shown that at mildly oxidizing potentials only small amounts of Pt are lost in the electrolyte solution [3–5]. Nonetheless, this treatment leads to a severely roughened electrode surface [6–9].

Experiments on well-defined single-crystal surfaces, specifically Pt(111), show that both the evolution of the surface structure as well as its electrochemical fingerprint are quite reproducible [10–13] and a theoretical model for the growth has been developed [14]. Although potential cycling experiments demonstrate that the roughening is determined by the oxidation and reduction of the surface, experiments resolving the structure of the oxidized surface are needed to gain more insight in the details of this process. Only a limited number of experimental techniques are suitable to perform such experiments, most notably surface X-ray diffraction (SXRD). Alternatively, direct imaging methods such as electrochemical scanning tunneling microscopy (EC-STM) could resolve details on the local atomic structure, although the electrochemical environment and the highly oxidizing potentials complicate high resolution measurements of the oxidized surface [15–18]. Spectroscopic measurements, on the other hand, provide important insights in the chemical composition of the oxide, but result in a comparison to bulk oxide structures rather than in a detailed structural description [19–23].

Although SXRD has been routinely applied for structure characterization, the relatively recent increased availability of high energy photons and large 2D detectors have boosted the possibili-

* Corresponding author.
E-mail addresses: leon.jacobse@desy.de (L. Jacobse), vedran.vonk@desy.de (V. Vonk), imccrum@clarkson.edu (I.T. McCrum), m.koper@lic.leidenuniv.nl (M.T.M. Koper), rost@physics.leidenuniv.nl (M.J. Rost), andreas.stierle@desy.de (A. Stierle).

https://doi.org/10.1016/j.electacta.2022.139881
0013-4686/

ties for in situ and operando studies [24–26]. First of all, employing X-ray photons with a high kinetic energy (20-100 keV) enable penetration of the complicated sample environments necessary for electrochemical experiments, while decreasing unwanted side reactions. Secondly, using 2D detectors, one can scan large parts of reciprocal space within a single detector image, bringing the timescale of the experiment down to minutes (compared to hours with a point detector) [24–26].

Previous in situ SXRD experiments on Pt(111) have mainly focused on the electrode roughening in potential cycling experiments [27–29]. In addition, experiments aiming at resolving the structure of the oxidized surface were performed as well [30–35]. These experiments have substantiated the hypothesis that the first step in the surface oxidation is the so-called place-exchange (PE) process, illustrated in Fig. 1. In the PE process, a Pt atom is lifted out of the topmost surface layer, without changing its in-plane lattice position (Pt*PE*, orange in Fig. 1). The formed vacancy site below the Pt*PE* atom is then occupied by an oxygen atom (O*PE*, dark red) that was previously adsorbed on the terrace. Although it is very challenging to resolve the oxygen atoms experimentally, several important insights are available from density functional theory (DFT) calculations. The most favorable adsorption site for subsurface oxygen is found to be the tetra-1 site, slightly offset from the original Pt lattice position as shown in Fig. 1 [36]. However, by in-plane coordination of additional O-species (light red in Fig. 1), Pt*PE* is also found to be stable without subsurface oxygen [37]. At higher oxygen coverages, a combination of these two geometries can occur, without changing much in the position of the Pt atoms. Finally, under electrochemical conditions, not only oxygen but also adsorbed water can lower the reaction barrier for the lifting of the Pt*PE* atom [38]. Here, we will use the nomenclature place-exchange to indicate Pt atoms that are lifted straight up from the surface without in plane displacement, independent from the exact position of the oxygen atom(s).

The PE process is relatively slow compared to the adsorption/desorption of H and OH occurring at lower potentials and therefore not considered electrochemically reversible. However, at least initially, it can be seen as structurally reversible in the sense that the smooth Pt(111) surface is recovered when the potential is decreased. Only when the potential is held sufficiently long in the oxidative regime, irreversible surface roughening occurs [12,33]. This suggests that a second, even slower, restructuring process is at play, e.g. a further surface oxidation or a reordering of the PE atoms. Importantly, only the topmost surface atoms are involved, as bulk oxidation does not yet occur at these potentials [39,40].

Pt oxide (super)structures, typically consisting of (reconstructed) oxide stripes, have been observed in gas-phase oxidation experiments on Pt(111) [41–43]. Although DFT calculations suggest that similar structures could also be stable under electrochemical conditions, they have, so far, not been observed experimentally [33,35,44]. As the stripe formation starts at rather low O_2 pressures, it seems unlikely that the maximum applied potential causes this discrepancy [45]. However, in the electrochemical SXRD experiments the potential is applied in a stepwise manner and the sample is at room temperature, such that kinetic barriers may drastically slow down the formation of the stripe structures [33,34]. Decreasing the oxidation rate by applying a very slow potential sweep rather than a potential step, increases the possibility for the formation of the thermodynamically most stable oxide structure (possibly the oxide superstructure) with the lowest free energy (thus still with disorder and dislocations).

Here, we analyze the structure of the oxidized Pt(111) surface resulting from slow potential sweeps and subsequent potential-hold experiments by high energy SXRD (HE-SXRD) experiments. Although we did not observe any hints of superstructure features, this experimental procedure leads to a significantly more ordered oxidized surface compared to potential step or cycling experiments using similar maximum potentials. Nonetheless, we find that beyond the reversible PE process, an irreversible regime is entered, where Pt surface atoms are displaced to positions that are not in registry with the underlying Pt(111) lattice. Although these atoms are 'invisible' in the diffraction signal, correlating these data to the voltammetry and the surface roughening provides us with insights on the resulting structure. Overall, this model helps understanding the full surface oxidation and reduction of Pt(111).

2. Experimental

In situ surface x-ray diffraction experiments were performed at the P07 beamline physics hutch, at the Deutsches Elektronen Synchrotron (DESY), employing a photon energy of 74.2 keV [46]. A Perkin Elmer XRD1621 2D detector with a pixel size of 200 × 200 μm^2 was used at a distance of 1500 mm from the sample. Lead absorber pieces were used to block the high intensity Bragg peaks, leading to gaps in the data at those positions.

The incidence angle was set at 0.03 degrees, close to the angle for external total reflection for Pt to improve the signal to noise ratio. A hexagonal surface unit cell (a=b=2.77 Å c=6.80 Å) was chosen such that the a* and b* reciprocal space vectors describe the surface plane while the c* vector lies along the surface normal. The corresponding H, K, and L coordinates were defined using a Pt lattice constant of 3.924 Å. Data processing [47], i.e. background subtraction, intensity correction, and signal integration, was performed using home-written scripts in Wavemetrics Igor Pro. The ANAROD package was used to fit the structural models to the data [48].

The used electrochemical cell allows for in situ SXRD experiments in an upside down hanging meniscus geometry as described elsewhere [49]. A syringe pump was used to control the electrolyte volume in the cell and thereby the meniscus size. All glassware and other parts of the setup that come into contact with the electrolyte were soaked for at least 24 h in a 1 g/L $KMnO_4$/0.5 M H_2SO_4 solution. Subsequently, the syringes and tubing of the syringe pump were flushed extensively with hot ultrapure water ($>18.2\ M\Omega \cdot cm$). All other parts were boiled at least five times in ultrapure water. The Pt(111) sample (cut and polished $< 0.1^\circ$) is prepared by repeated cycles of mild etching (± 2 V versus Pt, for 2.5 s at 50 Hz in an acidified $CaCl_2$ solution), flame annealing (5 min at ~1250 K), and cooling in a reducing atmosphere (1:4 H_2/Ar mixture). After the last cooling step, the surface is protected with ultrapure water, before it is mounted in the SXRD cell. Alignment of the sample is performed without electrolyte on the surface and while flushing the cell enclosure with Ar. High-purity perchloric acid (99.999% trace metals basis) is used to prepare the 0.1 M $HClO_4$ electrolyte solution. Several hours prior to and during the experiment, the electrolyte is purged with Ar. A miniaturized reversible hydrogen electrode (RHE) and a coiled Pt wire are used as reference and counter electrode, respectively. A potentiostat was used to control the potentials and collect the electrochemical data.

3. Results and discussion

3.1. Surface oxidation via place-exchange

First we will discuss results from our structural analysis using crystal truncation rod (CTR) experiments performed after slow sweep and hold experiments. CTRs are (weak) scattering rods in reciprocal space running perpendicular to the surface that originate from the broken periodicity at the interface between bulk and electrolyte. The shape of the CTR profile contains detailed information on the interface structure, specifically far away from the intense (bulk crystal) Bragg reflections [50]. This information can

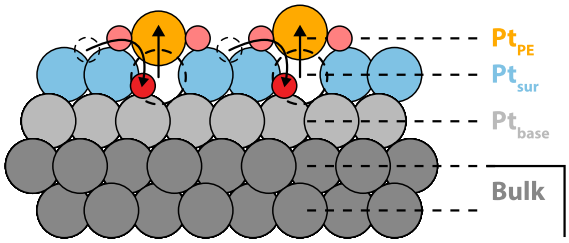

Fig. 1. The place-exchange model: In the PE process, a Pt atom from the surface layer (Pt*sur*) is lifted from the terrace without in-plane displacement [34], forming the PE layer (Pt*PE*). An oxygen atom (dark red) that was previously adsorbed on top of surface moves into the formed vacancy site. The subsurfa ce oxygen is generally thought to be bound at the tetra-1 site, i.e. right below the hcp surface site. The light red atoms indicate additional/alternative oxygen atoms that are usually present in the PE and oxide stripe structures. The vertical displacements are based on DFT calculations [37]. (For interpretation of the references to colour in this figure legend, the reader is referred to the web version of this article.)

be extracted by fitting model structures to the measured data. To study the surface oxidation in more detail, we drastically decreased the rate of oxidation compared to potential step [34] or sweep experiments in literature. In this experiment, we employed a potential scan rate of only 1 $mV\ s^{-1}$ and the potential was subsequently held for 30 min at 1.1, 1.2, 1.3, 1.4, and 1.5 V. During each potential hold, three subsequent SXRD measurements were performed, each containing the (1 1), (0 1), and (1 0) Crystal Truncation Rods (CTRs). Here, we analyze the last of the three measurements (started 20 min. after reaching the respective hold potential) quantitatively, as this represents the most equilibrated surface structure reached within our experiment. In our experiment, the intensity of the (1 0) CTRs is slightly attenuated for $L > 2$, possibly because of a slight misalignment of the sample. However, they are still shown, as they match (after applying a correction factor) very well with the fit results.

Figure 2 shows (in gray) the evolution of the (1 1), (0 1), and (1 0) CTRs at open circuit potential (OCP) and the different oxidizing potentials. Strong signal changes are observed during the experiment at the different hold potentials. The intermittent data, measured during the first 20 min, are provided in Fig. S1. Despite the very slow potential scan rate, it is clear that structural changes also occur at constant potential. However, those changes are relatively small compared to those induced by the increasing potential. A structural model describing the PE process and further disintegration of the surface structure due to oxidation was fitted to the data shown in Fig. 2. Oxygen atoms were omitted from this model as they lead to a negligible contribution to the CTR signal compared to the Pt atoms. For the Pt*sur* and Pt*PE* atoms, the displacement, occupancy, and anisotropic root mean square displacements (static Debye-Waller factors) were fitted. For the Pt*base* atoms, only the displacement were fitted, fixing the occupancy at unity and the thermal Debye-Waller factor at the bulk room temperature value of 0.38 [51]. Including an overall scale factor, this amounts to a total of ten fit parameters.

Initially, at the OCP, the CTR profiles can be fitted very well by an ideally bulk terminated surface, exhibiting a defect density below the resolution of our experiment ($< 1\%$, atomically smooth terraces). These results, including the very small outward relaxation of the Pt_{sur} layer, match perfectly with previous results [33,34]. At the oxidizing potentials applied here, the amount of Pt dissolving in the electrolyte during the surface oxidation is on the order of 1 mML, which is negligible for our analysis [5]. As a first attempt we have therefore used a mass conserved place exchange model to fit the data, i.e. the summed occupancy of Pt*sur* and Pt*PE* is fixed at unity. Although this model fits the shapes of the CTRs quite accurately (see Fig. S2-3), the interpretation is problematic, mainly because of the obtained occupancies. As Pt*PE* atoms are always adjacent to Pt*sur* atoms, even in the case of oxide row formation, there is a natural limit of the maximum Pt*PE* occupancy that is far below unity. The exact upper limit is unknown, but is expected to be in the 0.1-0.33 monolayer (ML) range, the latter being the maximum occupancy where no adjacent Pt*PE* sites can occur [52]. As can be seen in Fig. S3, a maximum PE occupancy of 0.8 ML is obtained at 1.5 V, leaving only 0.2 ML of the terrace unaffected, which is far beyond the expected upper limit and is thus unphysical. Simultaneously, we observe a drastic increase in the Debye-Waller factors at the highest potentials, especially for the Pt*PE* layer. As large Debye-Waller factors indicate a decreased contribution to the CTR intensity (see Fig. S10), it appears that the constraint of mass conservation leads to an overestimation of the occupancy of the Pt*PE* layer, which is then compensated by large Debye-Waller factors.

As a next step, to obtain a more consistent picture, we have tested a place exchange model without the mass-conservation constraint. The fits obtained in this approach are shown in Fig. 2 and the resulting parameter values in Fig. 3. For clarity, also the summed occupancy of Pt*sur* and Pt*PE* is shown in Fig. 3A, indicating a decrease in the number of atoms contributing to the CTR intensity. As the 'missing' atoms do not dissolve in the electrolyte [5], they must still reside on the surface, albeit at positions that are not in registry with the underlying Pt(111) lattice (i.e. from a disordered and/or incommensurate oxide [53], Pt*NR*), and thus do not contribute to the CTR signal. From Fig. 3 it is clear that the oxidation process still affects an increasing number Pt*sur* atoms with increasing potential. Initially, at 1.1 and 1.2 V most of these atoms are lifted into the Pt*PE* layer. Interestingly, the occupancy of the Pt_{PE} layer saturates now around 0.2 ML. This is within the regime expected for the PE process (see above) and close to the occupancy above which irreversible surface degradation was observed (0.15 ML) [33]. The improved description and quality of fit is not only reflected in a lower Pt*PE* occupancy, but also in a significantly lower Debye-Waller factor. The z-position of the Pt*PE* atoms (lifted slightly less than a monoatomic step height) is somewhat higher than the apparent height found by STM measurements in gas-phase oxidation experiments (1.7 Å above Pt*sur*), although this latter value has to be treated with caution due to the obviously different local density of states [42]. Furthermore, our values are close to those found in previous in situ SXRD studies [30,34]. The somewhat smaller vertical displacement of the Pt*PE* atoms at 1.1 V could possibly be related to the absence (and later formation) of subsurface oxygen [37]. Finally, also the χ^2 value improves with respect to the situation with the mass-conservation constraint (see Fig. S9). The decreasing number of the Pt*sur* atoms (in registry with the Pt(111) surface) with increasing potential indicates that the oxide exhibits a different periodicity and/or is partially disordered.

The dashed lines in Fig. 2 show calculations that were made using the (mass conserved) model and parameter values obtained by Ruge et al. from their potential step experiments at similar potentials (1.17 V, 1.37 V, and 1.57 V respectively) [34]. Immediately, it becomes clear that there is a significant difference in the measured structure factors and thus a difference in the formed surface structure between the potential step experiment and our slow sweep experiment. These differences are most prominent at the highest potentials in the (0 1) and (1 0) CTRs, whereas the differences at the lower potentials can most likely be attributed to the slightly different applied potentials. Intriguingly, in a potential step experiment, the CTRs measured under the most oxidative conditions resemble those of the pristine surface (except for the specular CTR, not shown here). This indicates the formation of a largely disordered oxide, where all the oxidized atoms no longer contribute to the CTR intensity. The large Debye-Waller factors for the Pt*PE* and

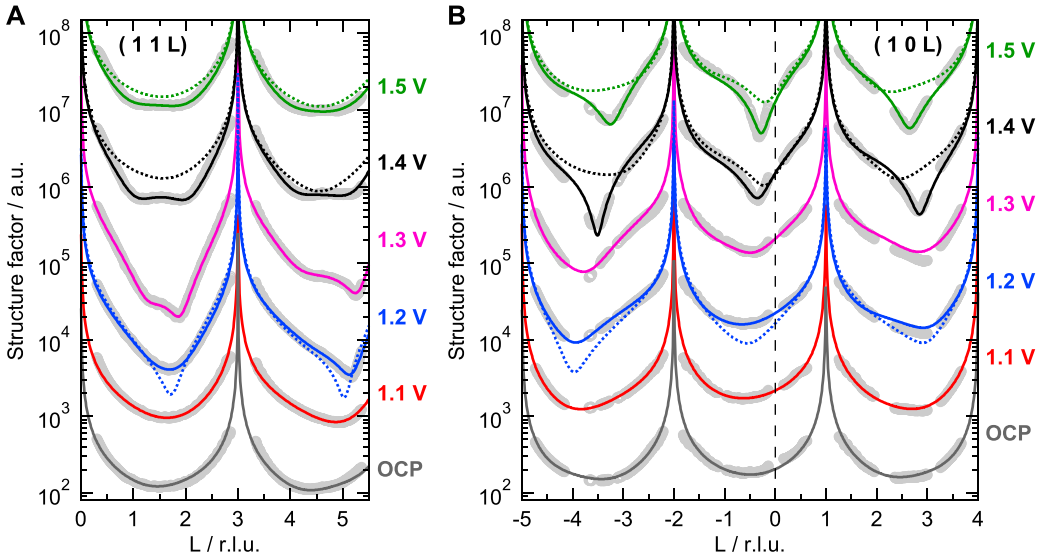

Fig. 2. Structure factors and fits: (A) (1 1) and (B) (0 1) and (1 0) CTR as a function of increasing potential. At each potential, the potential is kept constant for 30 min, during which three measurements are performed. Note that the (0 1 L) data is shown as (1 0 -L). The data of the last of those measurements are shown, vertically offset for clarity, in gray. The potential scan rate in between the measurements is 1 $mV\ s^{-1}$. The solid, colored lines are the best fits using the PE model (without mass conservation) shown schematically in Fig. 1. The values for the fit parameters are shown in Fig. 3. The dashed lines are calculations using the model and parameter values reported by Ruge et al. obtained in their potential step experiments [34]. Note that those data were measured at slightly different potentials (1.17, 1.37, and 1.57 for the blue, black, and green curve, respectively). Nonetheless, this comparison clearly demonstrates the differences that emerge at the highest potentials. (For interpretation of the references to colour in this figure legend, the reader is referred to the web version of this article.)

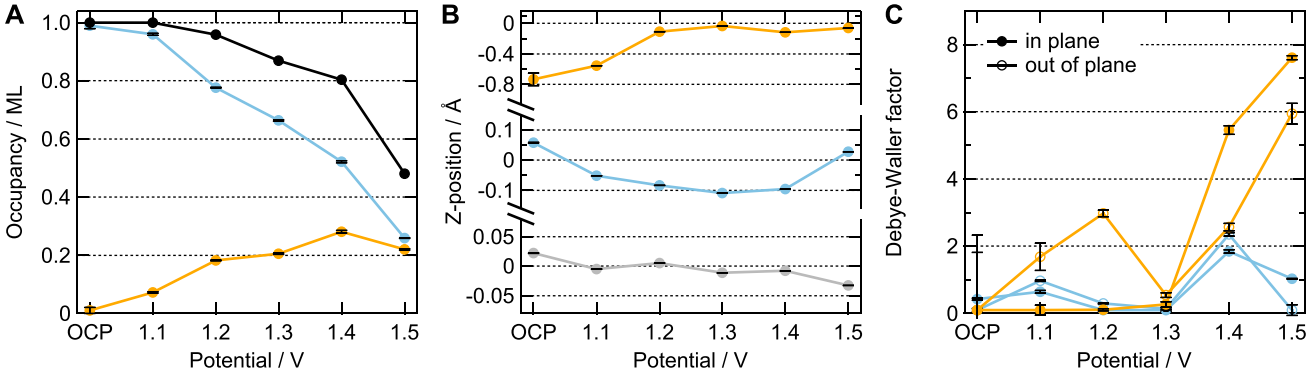

Fig. 3. Fit results: (A) Occupancies of the Pt*sur* (blue) and Pt*PE* (orange) layers as a function of sample potential. The summation of these two occupancies is shown in black. (B) Displacements of the Pt*base* (gray), Pt*sur* (blue), and Pt*PE* (orange) layers. Note that the y-axis is expanded to emphasize the differences and not the same for the different layers. The numbers indicate the displacement with respect to nearest atomic step height (see also Fig. 1). (C) In plane and out of plane Debye-Waller factors of the Pt*sur* (blue) and Pt*PE* (orange) layers. Note that the error bars only indicate the errors of the least-squares fit (see Fig. S9), whereas the real uncertainties may be larger (typically estimated at a few percent of the reported values. (For interpretation of the references to colour in this figure legend, the reader is referred to the web version of this article.)

Pt*sur* atoms (see also Fig. S3 and S10) confirm this. Note that we do know an oxide forms from the reduction voltammetry, the insignificant Pt dissolution [5], and the shape of the specular CTR reported in Ref. [34].

In our slow sweep experiment, strong minima are formed, making these CTRs distinctly different from those of the pristine surface. This means that under these conditions, the Pt*PE* and part of the surface atoms still contribute significantly to the measured signal. Thus, the formed oxide during the slow sweep retains much more of the Pt(111) order compared to the potential step experiment. Nonetheless, as lifting the constraint of mass conservation led to much more plausible values for the fit parameters, we conclude that this oxide is still partially disordered.

Although we cannot exactly determine the position of 0.5 ML of the displaced Pt atoms, lifting the mass conservation constraint allows us to determine the position of the Pt*PE* atoms with higher accuracy compared to the potential step experiments. This delivers important insights in the oxidation process and the surface roughening that occurs during potential cycling. After the formation of place exchange atoms, other Pt*sur* atoms are attacked by the oxidation process. We can also conclude that metallic adatom islands (as observed after reducing the surface [9,13]), or a commensurate α-PtO2 overlayer (as suggested by thermodynamical calculations [54], see Fig. S4) do not form. For the sake of completeness, simulated CTRs for such structures are provided in Fig. S5. A buckling model, involving an additional layer of lifted atoms, was used in an attempt to capture the additional displacements found in Kinetic Monte Carlo simulations on the extensive gas-phase oxidation of Pt(111) [55]. Although this model seems to provide an interesting lead (see Fig. S6-8), it also suffers from significantly increased Debye-Waller factors for the additional layer. Finally, we note that placing the lifted Pt atoms at other high-symmetry positions (i.e. fcc hollow, hcp hollow, and bridge sites) on top of

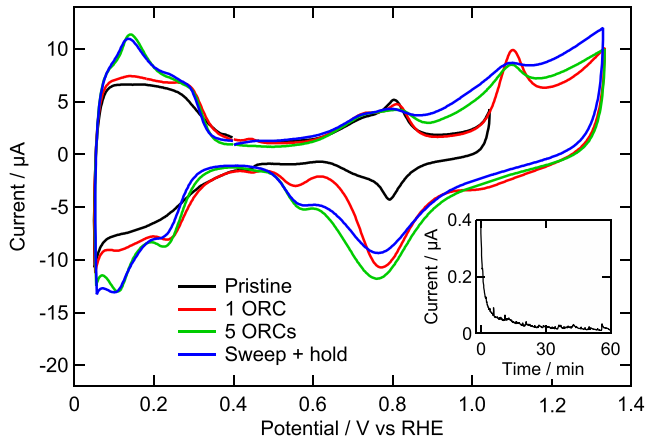

Fig. 4. Effect of oxidation method: CVs of the pristine surface (black) and measured after different oxidation experiments: one ORC (50 $mV\ s^{-1}$, between 0.04 and 1.35 V vs RHE, red), five ORCs (green), and one SH experiment (blue, 1 $mV\ s^{-1}$, between 0.04 and 1.35 V with a 60 min. potential hold at 1.35 V). All shown CVs are measured in the SXRD cell with a potential scan rate of 50 $mV\ s^{-1}$. The current during the potential hold of the SH experiment is shown in the inset. (For interpretation of the references to colour in this figure legend, the reader is referred to the web version of this article.)

the Pt*sur* layer, leads to a decrease in the fit quality, matching previous reports [33].

3.2. Surface oxidation dynamics

By combining the SXRD experiment with cyclic voltammetry, it is possible to extract more information on the surface oxidation dynamics and the chemical nature of the displaced atoms. In order to obtain this, the experimental procedure was slightly modified, keeping the potential scan rate of 1 $mV\ s^{-1}$, but pausing the potential sweep at only one value (1.35 V) for one hour. We will first discuss the electrochemical results before including the SXRD data, both starting from a freshly prepared sample.

Figure 4 shows cyclic voltammograms (CVs) of the Pt(111) electrode in 0.1 M $HClO_4$ measured in the SXRD cell. All shown CVs are recorded with a potential scan rate of 50 $mV\ s^{-1}$ after different oxidation experiments. The blue curve is a CV after a slow sweep and hold (SH) experiment, where the potential was scanned with 1 $mV\ s^{-1}$ and held at 1.35 V for 60 min. The red curve is a CV after a single oxidation–reduction cycle (ORC) between 0.04 and 1.35 V with a potential scan rate of 50 $mV\ s^{-1}$. Both CVs after oxidation contain contributions at potentials below 0.4 V (the H-adsorption region) that are not observed for the pristine surface (shown in black). These peaks are known to be related to the formation of specific 'defect' sites due to the surface roughening [13]. Clearly, the SH experiment leads to a much more increased roughness compared to a single ORC. Only after five ORCs (green curve in Fig. 4), the surface is roughened to the same extent as after one SH experiment. Interestingly, the different contributions of the H-adsorption region after one SH experiment and 5 ORCs overlap, indicating that in both cases the same distribution of defect-sites is obtained. Also the oxide reduction charge is increased, it is namely 2.5 times larger after the SH experiment compared to after one ORC (see Fig. S11). Apparently, the slower and longer oxidation in the SH experiment, has a much larger effect on the surface roughening (5 times larger) than on the amount of oxide formed (2.5 times larger). Actually, it is possible to apply potentials around 1.15 V during a CV, without (significant) surface roughening, whereas holding the potential for a few minutes at that same value leads to significant roughening [12,33]. This is an indication that the surface roughening is caused by a slow process, different from the (initial) PE process.

The inset of Fig. 4 displays the small oxidation current while the potential is held constantly at 1.35 V. This plot confirms that, even though the oxidation is executed with a slow potential scan rate, the surface is still further oxidized during the potential hold, like in the potential step experiment [33]. Matching literature data, the rate of oxidation decreases logarithmically during the potential hold [39], which leads to an almost negligible current after ~20 min.

In a separate SH experiment, we characterized the Pt(111) surface structure by fast measurements of the (0 1) CTR. Each of these CTR measurements took about 10 s, providing a potential resolution of 10 mV. Figure 5A shows a selection of the obtained (0 1) CTR structure factors as a function of potential and holding time. Initially, this profile matches that of the pristine Pt(111) surface. However, around 1.15 V, one can observe a small decrease in intensity, indicating a changing surface structure. The intensity decreases further during the remainder of the potential sweep up to 1.35 V. During the subsequent potential hold, the intensity decreases drastically, while the CTR also becomes strongly asymmetric around the Bragg peaks. After the first 20 min. of the potential hold, we observed only minimal changes in the CTR profile.

Again, the PE model, without mass conservation, was fitted to the CTR data. However, to avoid artefacts due the correlation between the occupancies and Debye-Waller factors, isotropic Debye-Waller factors were used and their values were fixed at either the bulk value, 1 (Pt*sur*), or 2 (Pt*PE*), based on the results above. This brings down the total number of fit parameters to six; two occupancies, three displacements, and the overall scaling factor. A selection of the fits is shown in Fig. 5B with the corresponding data. The resulting occupancies and displacements are shown in Fig. 6A and B, respectively. For clarity, also the summed occupancy of Pt*sur* and Pt*PE* is shown in black.

By following the evolution of the structure factor at surface sensitive positions in between the Bragg peaks during the potential sweep (see Fig. S12), we have determined the onset of the surface oxidation process to be at 1.05 V, matching previous results [29,32,33,56]. Indeed, above this potential an increase (decrease) in the number of Pt*PE* (Pt*sur*) atoms is observed. At slightly higher potentials, we observe a decrease in the total occupancy, indicating the formation of Pt*NR*. After reaching the upper potential limit of the sweep (1.35 V, indicated by the vertical dashed line), the Pt*PE* occupancy saturates around 0.2 ML within three minutes. The occupancy of Pt*sur*, on the other hand, decreases an additional 0.15 ML during the subsequent 15–20 min. This must also lead to a decrease in the summed occupancy, once more indicating a slow oxidation process where Pt*sur* atoms are moved to out of registry positions. The vertical displacements of the Pt*PE* are similar to those observed during the SH experiment, slightly less than a monoatomic step height. Again, we also observe a smaller displacement near the onset of the PE process, although this effect is now less pronounced.

Figure 6C shows the correlation between the total number of displaced Pt atoms (Pt_{lift}=Pt*PE*+Pt*NR*) and the cumulative oxidation charge measured during the potential sweep (above 1 V, red) and hold (blue). The number of displaced Pt atoms is determined from the occupancy of Pt*sur*. As expected, both signals are related to the surface oxidation, a strong correlation is observed. Initially, this correlation indicates that slightly more than four electrons are involved in the formation of each Pt_{lift} site as shown by the solid line in Fig. 6C. Note that the oxidation charge is slightly overestimated as the data is not corrected for the capacitive current due to charging of the electrochemical double layer. The value of 4 e^-/Pt_{lift}, suggests that for each Pt atom lifted out of the surface, two additional oxygen atoms are bound. For the Pt*PE* layer, this

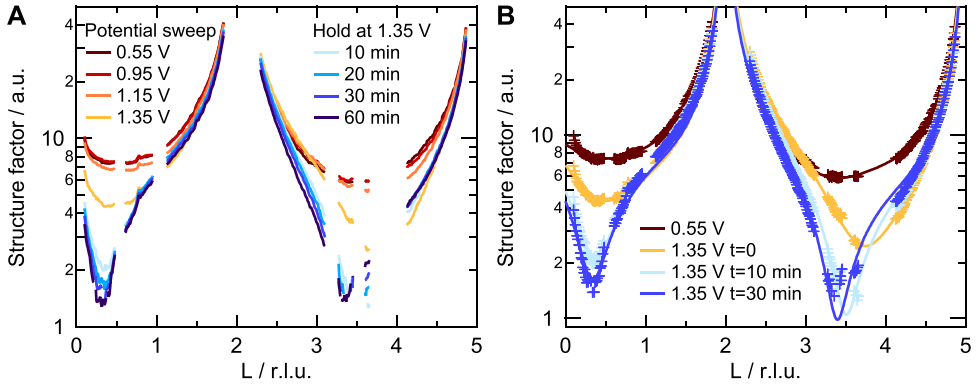

Fig. 5. Surface evolution: (A) (0 1) CTRs measured while sweeping the potential (1 $mV\ s^{-1}$) up to 1.35 V vs RHE and subsequently holding it. (B) (0 1) CTRs measured at 0.55 V, 1.35 V, and at 1.35 V after holding the potential for 10 and 30 min (markers) and the corresponding fits (solid lines).

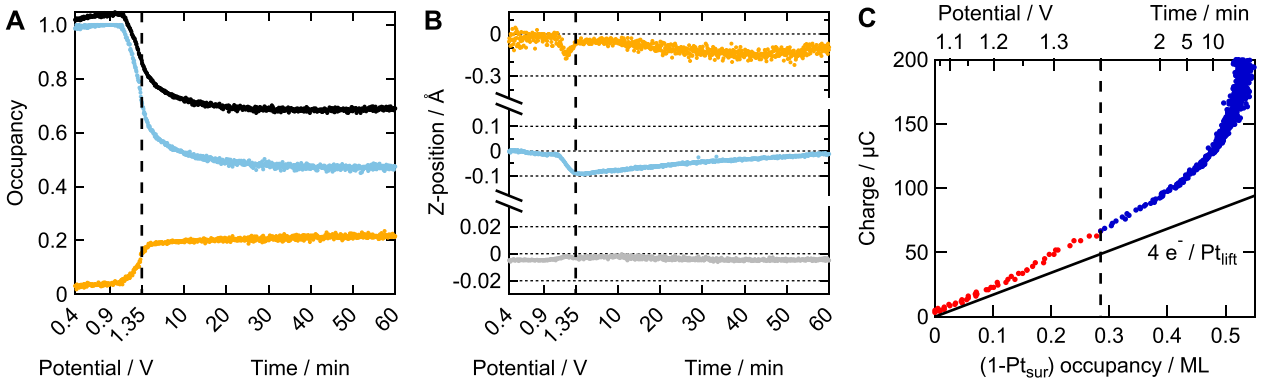

Fig. 6. PE evolution: (A) Occupancies of the Pt*PE* and Pt*sur* layers obtained by fitting the (0 1) CTR as a function of potential and time. The summation of these two occupancies is shown in black. (B) Displacements of the Pt*base* (gray), Pt*sur* (blue), and Pt*PE* (orange) layers. Note that the y-axis is expanded to emphasize the differences and not the same for the different layers. The numbers indicate the displacement with respect to nearest atomic step height (see also Fig. 1). (C) Correlation between the number of displaced Pt atoms and the oxidation charge from the slow potential sweep (red, above 1 V) and the potential hold (blue). The solid line indicates a slope corresponding to four transferred electrons for each Pt_{lift}. Note that this plot is not linear in time. (For interpretation of the references to colour in this figure legend, the reader is referred to the web version of this article.)

matches with two in-plane oxygen atoms bound to the Pt*PE* atoms [37,44]. Specifically, this indicates that also the Pt*NR* atoms are oxidized. We conclude this from the fact that the number of Pt*PE* atoms is less than half of the total number of displaced atoms. If only the Pt*PE* atoms would be oxidized, the formation of each of those atoms should lead to the transfer of ~10 electrons, which is unrealistically high. Importantly, this confirms that the metallic adatom islands observed for the reduced surface [9], do not already form during the oxidation process, although it does not rule out the nucleation of these islands during the oxidation in the form of Pt-oxide clusters. During the potential hold, especially after more than 10 min, the slope deviates more and more from the 4 e^-/Pt_{lift} line. From Fig. 5A it is clear that at this point the surface oxidation rate has decreased to practically zero, and thus cannot be responsible for the observed steady state current. Although the nature of this current is currently not fully clear, oxygen evolution seems the most plausible explanation, as this reaction becomes significant around the holding potential [23]. Such a (catalytic) process eventually leads to a vertical asymptote in Fig. 6C.

3.3. Reduction and roughening

After holding the potential for 60 min, the potential was decreased again to reduce the surface. Figure 7A shows (light blue markers) the (0 1) CTR for the fully reduced surface at 0.4 V. Clearly, the strong asymmetry and the deep minima of the CTR seen for the oxidized surface, has disappeared. Nonetheless, the intensity does not fully recover to that of the pristine surface, demonstrating the irreversible surface roughening. If the electrode is subsequently subjected to a series of ORCs (i.e. 50 $mV\ s^{-1}$ cycling up to 1.35 V without holding the potential), this intensity decreases further, as is shown with the dark blue markers. The inset of Fig. 7A shows the evolution of the intensity at (0 1 1.5) as a function of the ORC number, measured in a potential cycling experiment. The full CTRs are shown in Fig. S12. A model using only an intensity scaling and a surface roughness (Poisson distribution) parameter was used to analyze these data (fits shown in Fig. S12), providing the root mean square roughness of the surface. Fig. 7B shows the resulting values (blue) together with values that were previously determined from EC-STM experiments (red) [9]. The increase in roughness with increasing ORC number corresponds very well between these two sets of data. The vertical offset can be explained from the convolution between the EC-STM tip and the rough surface, which leads to an underestimation of the RMS roughness in these experiments [9,13]. The surface roughness after the SH experiment (after reduction, measured at 0.4 V) is similar to that after 4–5 ORCs (as obtained by interpolation), which matches with the observations from the voltammetry.

Finally, it is interesting to see if the amount of roughness generated for the reduced surface can be understood from the occupancies found for the oxidized surface. At the end of the SH experiment, the occupancy of Pt*PE*, and Pt*sur* are 0.21 and 0.47, respectively. As was discussed above, it is likely that upon reduction the Pt*PE* atoms return to their original lattice positions, whereas the Pt*NR* atoms contribute to the surface roughening. If all Pt*NR*

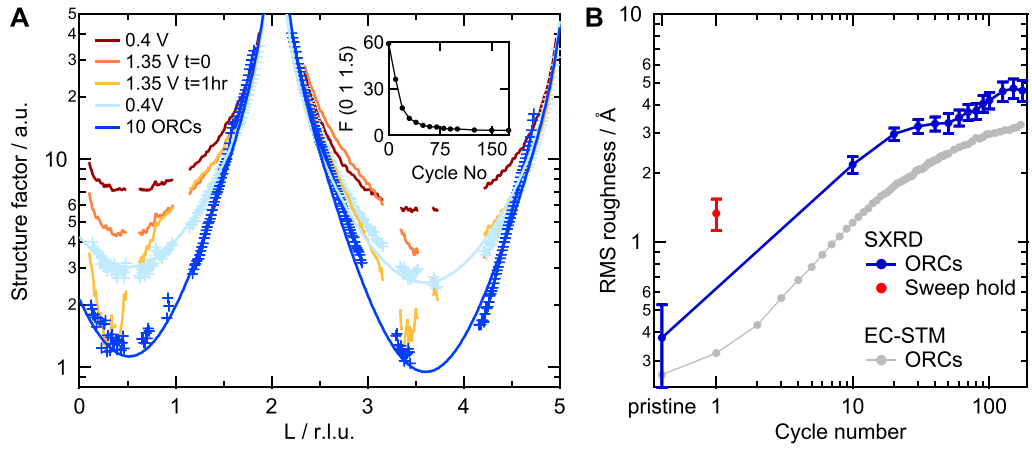

Fig. 7. Reduction and potential cycling: (A) (0 1) CTRs during oxide formation and reduction and subsequent potential cycling (up to 1.35 V vs RHE, with a scan rate of 50 $mV\ s^{-1}$). The inset shows the structure factor at (0 1 1.5) as a function of ORC number. (B) RMS roughness evolution as function of ORC number. The blue data are determined from the SXRD potential cycling experiment. The gray data are EC-STM literature data from an experiment using the same potential cycling conditions [9]. The red point indicates the roughness created during the SH experiment. All data were measured at the reduced surface, at a potential of 0.4 V. (For interpretation of the references to colour in this figure legend, the reader is referred to the web version of this article.)

atoms form adatom islands of monoatomic height, those islands would cover 1-(Pt*PE*+Pt*sur*)=0.32 ML of the surface and the same amount of vacancies must be formed as well. From these occupancies, one can calculate the RMS roughness to be 1.8 Å, which is quite a bit larger than the 1.3 Å found in Fig. 7B. From the reverse calculation, we find that the RMS roughness of 1.3 Å corresponds to an adatom (and vacancy) coverage of 0.16 ML. This indicates that approximately half of the Pt*NR* atoms still return into the terrace once the surface is reduced. Note that this is only a very rough indication, as dissolution (which occurs to a small extent during the reduction [5]), as well as the possibility of atoms being incorporated into a step edge are not taken into account. Nonetheless, the adatom coverage of 0.16 ML is, corrected for the above-mentioned factor 4–5, close to the 0.0245 ML/ORC that was found with the theoretical growth model [14].

3.4. Absence of oxide superstructure

Summarizing, we have shown that, as expected, the surface oxidation starts with the PE process around 1.05 V. Within a potential interval of 100–150 mV (see Fig. 3), however, a second oxidation process leads to the formation of a disordered oxide. The PE process reaches a steady state at around 1.2 V (due to the slow reaction kinetics, changes are observed up to 1.35V in the SH experiment). Upon reduction, most of the displaced atoms return to their original positions, as the generated surface roughness is much smaller than expected from the summed occupancies of Pt*PE* and Pt*NR*. Considering that the PE process is reversible and that the Pt*NR* atoms undergo larger displacements, we conclude that the latter are responsible for the surface roughening that occurs during potential cycling. In our SH experiment, approximately half of the formed Pt*NR* atoms, ends up in adatom islands after reduction of the surface.

In another scenario, the formation of an ordered oxide (super)structure could explain the above observations as well as the adatom island nucleation [52]. Several structures have previously been observed in gas-phase oxidation experiments on Pt(111), typically in the form of oxide stripes [41–43]. These stripes can be seen as rows of Pt*PE* atoms, coordinated by in-plane oxygen atoms, locally resembling a PtO_2 phase. However, the Pt-Pt distances along the stripes are strongly compressed compared to $\alpha - PtO_2$, the thermodynamically most stable Pt oxide under these conditions. The resulting stress is the driving force for the removal of one Pt atom from the stripe, leading to the formation of oxide superstructures [43]. DFT calculations suggest that such superstructures, sometimes hexagonally ordered in so-called spoked wheel structures, could also form under electrochemical conditions [44]. These calculations indicate that stripes containing seven elevated Pt atoms spread across eight surface lattice positions (7/8-stripes) are most likely to form.

When the superstructure stripes/spokes form, by connecting previously isolated Pt*PE* atoms, atoms have to expelled from the stripe/spoke and the remaining PE atoms undergo large in-plane displacements such that some no longer contribute to the CTR intensity. Additionally, there are the atoms that need to be expelled from the stripes. As also these atoms are oxidized (see Fig. 6C), they do not necessarily end up at regular lattice positions. Upon reduction, one could expect that the atoms within the stripe fall back in the terrace, whereas the expelled atoms form the adatom islands.

If a superstructure would form under electrochemical conditions, this should lead to the appearance of a signal at a different position on the detector, i.e. a different in-plane momentum transfer ($q_{\parallel} \propto \sqrt{H^2 + K^2}$). Figure 8 shows a stacked (by maximum intensity) detector image from a (0 1) CTR measurement taken at the end of the SH experiment, i.e. after holding the potential at 1.35 V for 60 min. The bottom panel shows an in-plane line profile extracted from the detector images at L=0.8 (indicated by the white dashed line). From simulations of the 7/8-stripes structure (see Fig. S13), we know that this experiment should capture one of the most intense features due to these structures. Specifically, one would expect a surface rod running parallel to the (0 1) CTR at $q_{\parallel}$=2.29 $Å^{-1}$ indicated by the blue dashed arrow. From both the stacked detector image as well as the extracted line profile, it is clear that there are no indications for the formation of the 7/8-stripes. Note that, based on the rather large amount of expelled atoms (0.16 ML as discussed above), one might expect somewhat shorter stripes. However, such signals (similar surface rods, but at smaller $q_{\parallel}$) are also absent in the data. Also in all our experiments as well as in literature [33], there are no superstructure features detectable. Furthermore, there are also no signs of diffuse scattering around the CTR signals, as could be expected for the formation of a 3D bulklike disordered oxide [33]. This confirms that the formed oxide is 2D in nature, i.e. limited to the surface layer.

Whereas the appearance of a superstructure rod would be hard proof of the existence of such a structure, the opposite is not nec-

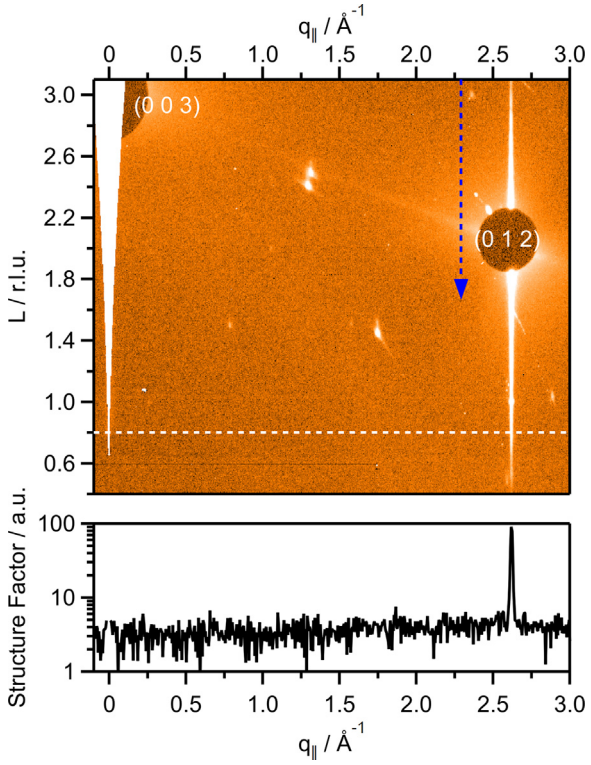

Fig. 8. Ordered oxide: the maximum intensity from a series of detector images from a (0 1) CTR measurement after applying 1.35 V for 60 min. The blue dashed line indicates the $q_{\parallel}$ value where a signal due to the formation of 7/8-stripes would appear. The white dashed line indicates the L-value which was used to extract the profile shown in the bottom panel. (For interpretation of the references to colour in this figure legend, the reader is referred to the web version of this article.)

essarily true. If the stripes form only small ordered domains [43] or if they do not exhibit any ordering between themselves at all, they would be difficult to observe in a diffraction-based experiment. On the other hand, it is also possible that the oxide stripes do indeed not form. In that case, one might expect a rather disordered surface oxide, such as found in Kinetic Monte Carlo simulations on the gas-phase oxidation of Pt(111) [55]. Here, the oxidation also starts with the PE process, but at oxygen coverages beyond 0.56 ML, Pt atoms are displaced in both the in-plane and out of plane directions. Although higher resolution, atomically-resolved, data are required to draw hard conclusions, EC-STM experiments seem to point in this direction [15].

4. Conclusions

The oxidation and subsequent reduction of Pt(111) electrodes leads to a severe surface roughening. Although this roughening has been described in detail, much less is known about the underlying cause, i.e. the structure of the electrochemically formed oxide. The place-exchange mechanism provides a good model to describe the initial reversible surface oxidation, but is limited to rather low coverages of lifted Pt atoms and does not explain the surface roughening. We have used in situ HE-SXRD measurements to study the Pt(111) surface oxidation employing very slow oxidation rates. This approach leads to a more ordered oxidized surface compared to previous potential step or sweep experiments. This increased surface order allows to disentangle two processes relevant for the initial electrochemical oxidation of Pt, which was impossible in previous experiments. Thereby, our results provide important insights in the oxidation process of Pt(111) beyond the reversible PE process. After formation of place exchanged atoms up to the physical limit, other surface atoms get attacked by oxidation and leave the regular Pt(111) surface lattice site. We demonstrate that during this oxidation process, about 20% of the surface atoms sits on place-exchange sites, whereas 30% remain on regular surface sites. The remaining 50% of the atoms are incorporated in the disordered oxide. A possible explanation for these results is the formation of short reconstructed oxide stripes or spokes. However, the absence of the expected diffraction signal indicates a more disordered surface and large, ordered superstructure domains can be excluded. Complementary atomically-resolved imaging experiments would be beneficial to find out if smaller domains do form or if the oxidized surface is even more disordered. Additional experiments, e.g. X-ray absorption and/or specular CTR measurements could provide valuable further information on the structure and composition of the disordered oxide.

The differences between the structures depending on the potential scan rate could help designing experimental procedures that decrease the electrode degradation. Extending this knowledge further, e.g. to potentials where bulk oxidation and even oxygen evolution occur, will be beneficial for understanding the degradation of Pt electrodes under operando conditions. Our results can serve as important input for future studies by theory and experiment to finally disentangle the atomic structure of the Pt oxide formed under electrochemical conditions.

Declaration of Competing Interest

The authors declare that they have no known competing financial interests or personal relationships that could have appeared to influence the work reported in this paper.

Acknowledgments

This work is part of the research programme TOP with project number 716.017.001, which is financed by The Netherlands Organisation for Scientific Research (NWO). This project has received funding from the EU-H2020 research and innovation programme under grant agreement No 654360 having benefitted from the access provided by Deutsches Elektronen Synchrotron DESY in Hamburg, Germany within the framework of the NFFA-Europe Transnational Access Activity. We acknowledge DESY (Hamburg, Germany), a member of the Helmholtz Association HGF, for the provision of experimental facilities. Parts of this research were carried out at PETRA III and we would like to thank Olof Gutowski and Ann-Christin Dippel for assistance in using the High Energy Materials Science Beamline (P07). Beamtime was allocated for proposal 20010107 (NFFA).

Supplementary material

Supplementary material associated with this article can be found, in the online version, at doi:10.1016/j.electacta.2022.139881.

References

[1] J.C. Meier, C. Galeano, I. Katsounaros, J. Witte, H.J. Bongard, A.A. Topalov, C. Baldizzone, S. Mezzavilla, F. Schüth, K.J.J. Mayrhofer, Design criteria for stable Pt/C fuel cell catalysts, Beilstein J. Nanotechnol. 5 (1) (2014) 44–67, doi:10.3762/bjnano.5.5.

[2] T.F. Keller, S. Volkov, E. Navickas, S. Kulkarni, V. Vonk, J. Fleig, A. Stierle, Nanoscale oxide formation inside electrochemically-formed Pt blisters at a solid electrolyte interface, Solid State Ionics 330 (2019) 17–23, doi:10.1016/j.ssi.2018.11.009.

[3] A.A. Topalov, I. Katsounaros, M. Auinger, S. Cherevko, J.C. Meier, S.O. Klemm, K.J. Mayrhofer, Dissolution of platinum: limits for the deployment of electrochemical energy conversion? Angew. Chemie - Int. Ed. 51 (50) (2012) 12613–12615, doi:10.1002/anie.201207256.

[4] P.P. Lopes, D. Strmcnik, D. Tripkovic, J.G. Connell, V.R. Stamenkovic, N.M. Markovic, Relationships between atomic level surface structure and stability/activity of platinum surface atoms in aqueous environments, ACS Catal. 6 (4) (2016) 2536–2544, doi:10.1021/acscatal.5b02920.

[5] D.J. Sandbeck, O. Brummel, K.J. Mayrhofer, J. Libuda, I. Katsounaros, S. Cherevko, Dissolution of platinum single crystals in acidic medium, Chemphyschem 20 (22) (2019) 2997–3003, doi:10.1002/cphc.201900866.

[6] I. Khalakhan, A. Choukourov, M. Vorokhta, P. Kúš, I. Matolínová, V. Matolín, In situ electrochemical AFM monitoring of the potential-dependent deterioration of platinum catalyst during potentiodynamic cycling, Ultramicroscopy 187 (2018) 64–70, doi:10.1016/j.ultramic.2018.01.015.

[7] X. Deng, F. Galli, M.T. Koper, In situ electrochemical AFM imaging of a pt electrode in sulfuric acid under potential cycling conditions, J. Am. Chem. Soc. 140 (41) (2018) 13285–13291, doi:10.1021/jacs.8b07452.

[8] N. Arulmozhi, D. Esau, R.P. Lamsal, D. Beauchemin, G. Jerkiewicz, Structural transformation of monocrystalline platinum electrodes upon electrooxidation and electro-dissolution, ACS Catal. 8 (7) (2018) 6426–6439, doi:10.1021/acscatal.8b00319.

[9] L. Jacobse, Y.-F.F. Huang, M.T.M. Koper, M.J. Rost, Correlation of surface site formation to nanoisland growth in the electrochemical roughening of Pt(111), Nat. Mater. 17 (3) (2018) 277–282, doi:10.1038/s41563-017-0015-z.

[10] N. Furuya, M. Shibata, Structural changes at various pt single crystal surfaces with potential cycles in acidic and alkaline solutions, J. Electroanal. Chem. 467 (1) (1999) 85–91, doi:10.1016/S0022-0728(99)00077-7.

[11] A. Bjorling, J.M. Feliu, Electrochemical surface reordering of Pt(111): a quantification of the place-exchange process, J. Electroanal. Chem. 662 (1) (2011) 17–24, doi:10.1016/j.jelechem.2011.01.045.

[12] A.M. Gómez-Marín, J.M. Feliu, Pt(1 1 1) surface disorder kinetics in perchloric acid solutions and the influence of specific anion adsorption, Electrochim. Acta 82 (2012) 558–569, doi:10.1016/j.electacta.2012.04.066. Pergamon

[13] L. Jacobse, M.J. Rost, M.T.M. Koper, Atomic-scale identification of the electrochemical roughening of platinum, ACS Cent. Sci. 5 (12) (2019) 1920–1928, doi:10.1021/acscentsci.9b00782.

[14] M.J. Rost, L. Jacobse, M.T. Koper, The dualism between adatom- and vacancy-based single crystal growth models, Nat. Commun. 10 (1) (2019) 5233, doi:10.1038/s41467-019-13188-0.

[15] M. Wakisaka, S. Asizawa, H. Uchida, M. Watanabe, In situ STM observation of morphological changes of the Pt(111) electrode surface during potential cycling in 10 mm HF solution, Phys. Chem. Chem. Phys. 12 (16) (2010) 4184–4190, doi:10.1039/B923956A.

[16] M.J. Rost, High-speed electrochemical STM, in: K. Wandelt (Ed.), Encyclopedia of Interfacial Chemistry, Elsevier, 2018, pp. 180–198, doi:10.1016/b978-0-12-409547-2.13622-4.

[17] X. Gao, M.J. Weaver, Nanoscale structural changes upon electro-oxidation of Au(111) as probed by potentiodynamic scanning tunneling microscopy, J. Electroanal. Chem. 367 (1–2) (1994) 259–264, doi:10.1016/0022-0728(93)03263-O.

[18] Y.I. Yanson, F. Schenkel, M.J. Rost, Design of a high-speed electrochemical scanning tunneling microscope, Rev. Sci. Instrum. 84 (2) (2013) 023702, doi:10.1063/1.4779086.

[19] M. Wakisaka, H. Suzuki, S. Mitsui, H. Uchida, M. Watanabe, Identification and quantification of oxygen species adsorbed on Pt(111) single-crystal and polycrystalline pt electrodes by photoelectron spectroscopy, Langmuir 25 (4) (2009) 1897–1900, doi:10.1021/la803050r.

[20] H. Imai, K. Izumi, M. Matsumoto, Y. Kubo, K. Kato, Y. Imai, In situ and real-time monitoring of oxide growth in a few monolayers at surfaces of platinum nanoparticles in aqueous media, J. Am. Chem. Soc. 131 (17) (2009) 6293–6300, doi:10.1021/ja810036h.

[21] Y.-F. Huang, P.J. Kooyman, M.T.M. Koper, Intermediate stages of electrochemical oxidation of single-crystalline platinum revealed by in situ raman spectroscopy, Nat. Commun. 7 (2016) 12440, doi:10.1038/ncomms12440.

[22] F. Sugimura, N. Sakai, T. Nakamura, M. Nakamura, K. Ikeda, T. Sakai, N. Hoshi, In situ observation of pt oxides on the low index planes of Pt using surface enhanced raman spectroscopy, Phys. Chem. Chem. Phys. 19 (40) (2017) 27570–27579, doi:10.1039/C7CP04277A.

[23] F. Bizzotto, H. Ouhbi, Y. Fu, G.K. Wiberg, U. Aschauer, M. Arenz, Examining the structure sensitivity of the oxygen evolution reaction on Pt single-crystal electrodes: a combined experimental and theoretical study, Chemphyschem 20 (22) (2019) 3154–3162, doi:10.1002/cphc.201900193.

[24] J. Gustafson, M. Shipilin, C. Zhang, A. Stierle, U. Hejral, U. Ruett, O. Gutowski, P.A. Carlsson, M. Skoglundh, E. Lundgren, High-energy surface x-ray diffraction for fast surface structure determination, Science 343 (6172) (2014) 758–761, doi:10.1126/science.1246834.

[25] G.S. Harlow, E. Lundgren, M. Escudero-Escribano, Recent advances in surface x-ray diffraction and the potential for determining structure-sensitivity relations in single-crystal electrocatalysis, Curr. Opin. Electrochem. 23 (2020) 162–173, doi:10.1016/j.coelec.2020.08.005.

[26] U. Hejral, M. Shipilin, J. Gustafson, A. Stierle, E. Lundgren, High energy surface x-ray diffraction applied to model catalyst surfaces at work, J. Phys. Condens. Matter (2021), doi:10.1088/1361-648x/abb17c.

[27] H. You, Z. Nagy, Oxidation–reduction-induced roughening of platinum (111) surface, Phys. B Condens. Matter 198 (1–3) (1994) 187–194, doi:10.1016/0921-4526(94)90157-0.

[28] Z. Nagy, H. You, Applications of surface x-ray scattering to electrochemistry problems, Electrochim. Acta 47 (19) (2002) 3037–3055, doi:10.1016/S0013-4686(02)00223-2.

[29] M. Ruge, J. Drnec, B. Rahn, F. Reikowski, D.A. Harrington, F. Carlà, R. Felici, J. Stettner, O.M. Magnussen, Structural reorganisation of Pt(111) electrodes by electrochemical oxidation and reduction, J. Am. Chem. Soc. 139 (12) (2017) 4532–4539, doi:10.1021/jacs.7b01039.

[30] H. You, D.J. Zurawski, Z. Nagy, R.M. Yonco, In-situ x-ray reflectivity study of incipient oxidation of Pt(111) surface in electrolyte solutions, J. Chem. Phys. 100 (6) (1994) 4699, doi:10.1063/1.466254.

[31] I.M. Tidswell, N.M. Markovic, P.N. Ross, Potential dependent surface structure of the Pt(1 1 1) electrolyte interface, J. Electroanal. Chem. 376 (1–2) (1994) 119–126, doi:10.1016/0022-0728(94)03553-9.

[32] Y. Liu, A. Barbour, V. Komanicky, H. You, X-ray crystal truncation rod studies of surface oxidation and reduction on Pt(111), J. Phys. Chem. C 120 (29) (2016) 16174–16178, doi:10.1021/acs.jpcc.6b00492.

[33] J. Drnec, M. Ruge, F. Reikowski, B. Rahn, F. Carlà, R. Felici, J. Stettner, O.M. Magnussen, D.A. Harrington, Initial stages of Pt(111) electrooxidation: dynamic and structural studies by surface x-ray diffraction, Electrochim. Acta 224 (2017) 220–227, doi:10.1016/j.electacta.2016.12.028.

[34] M. Ruge, J. Drnec, B. Rahn, F. Reikowski, D.A. Harrington, F. Carlà, R. Felici, J. Stettner, O.M. Magnussen, Electrochemical oxidation of smooth and nanoscale rough Pt(111): an in situ surface x-ray scattering study, J. Electrochem. Soc. 164 (9) (2017) H608–H614, doi:10.1149/2.0741709jes.

[35] T. Fuchs, J. Drnec, F. Calle-Vallejo, N. Stubb, D.J. Sandbeck, M. Ruge, S. Cherevko, D.A. Harrington, O.M. Magnussen, Structure dependency of the atomic-scale mechanisms of platinum electro-oxidation and dissolution, Nat. Catal. (2020) 1–8, doi:10.1038/s41929-020-0497-y. https://doi.org/10.1038/s41929-020-0497-y

[36] J.M. Hawkins, J.F. Weaver, A. Asthagiri, Density functional theory study of the initial oxidation of the Pt(111) surface, Phys. Rev. B - Condens. Matter Mater. Phys 79 (12) (2009), doi:10.1103/PhysRevB.79.125434.

[37] D. Fantauzzi, J.E. Mueller, L. Sabo, A.C. Van Duin, T. Jacob, Surface buckling and subsurface oxygen: atomistic insights into the surface oxidation of Pt(111), Chemphyschem 16 (13) (2015) 2797–2802, doi:10.1002/cphc.201500527.

[38] M.J. Eslamibidgoli, M.H. Eikerling, Atomistic mechanism of pt extraction at oxidized surfaces: insights from DFT, Electrocatalysis 7 (4) (2016) 345–354, doi:10.1007/s12678-016-0313-2.

[39] B.E. Conway, G. Jerkiewicz, Surface orientation dependence of oxide film growth at platinum single crystals, J. Electroanal. Chem. 339 (1–2) (1992) 123–146, doi:10.1016/0022-0728(92)80448-D.

[40] T. Löffler, R. Bussar, X. Xiao, S. Ernst, H. Baltruschat, The adsorption of ethene on vicinally stepped electrode surfaces and the effect of temperature, J. Electroanal. Chem. 629 (1–2) (2009) 1–14, doi:10.1016/j.jelechem.2008.12.024.

[41] C. Ellinger, A. Stierle, I.K. Robinson, A. Nefedov, H. Dosch, Atmospheric pressure oxidation of Pt(111), J. Phys. Condens. Matter 20 (18) (2008) 184013, doi:10.1088/0953-8984/20/18/184013.

[42] S.P. Devarajan, J.A. Hinojosa, J.F. Weaver, STM study of high-coverage structures of atomic oxygen on Pt(1 1 1): P(2-1) and Pt oxide chain structures, Surf. Sci. 602 (19) (2008) 3116–3124, doi:10.1016/J.SUSC.2008.08.008.

[43] M.A. van Spronsen, J.W.M. Frenken, I.M.N. Groot, Observing the oxidation of platinum, Nat. Commun. 8 (1) (2017) 429, doi:10.1038/s41467-017-00643-z.

[44] S. Hanselman, I.T. McCrum, M.J. Rost, M.T.M. Koper, Thermodynamics of the formation of surface PtO2 stripes on Pt(111) in the absence of subsurface oxygen, Phys. Chem. Chem. Phys. (2020), doi:10.1039/c9cp05107d.

[45] D.J. Miller, H. Øberg, S. Kaya, H. Sanchez Casalongue, D. Friebel, T. Anniyev, H. Ogasawara, H. Bluhm, L.G. Pettersson, A. Nilsson, Oxidation of Pt(111) under near-ambient conditions, Phys. Rev. Lett. 107 (19) (2011) 195502, doi:10.1103/PhysRevLett.107.195502.

[46] N. Schell, A. King, F. Beckmann, T. Fischer, M. Müller, A. Schreyer, The high energy materials science beamline (HEMS) at PETRA III, Mater. Sci. Forum 772 (2014) 57–61.

[47] M. Shipilin, U. Hejral, E. Lundgren, L.R. Merte, C. Zhang, A. Stierle, U. Ruett, O. Gutowski, M. Skoglundh, P.-A. Carlsson, J. Gustafson, Quantitative surface structure determination using in situ high-energy SXRD: surface oxide formation on Pd(100) during catalytic CO oxidation, Surf. Sci. 630 (2014) 229–235, doi:10.1016/j.susc.2014.08.021.

[48] E. Vlieg, ROD: a program for surface x-ray crystallography, J. Appl. Crystallogr. 33 (2) (2000) 401–405, doi:10.1107/S0021889899013655.

[49] O.M. Magnussen, K. Krug, A.H. Ayyad, J. Stettner, In situ diffraction studies of electrode surface structure during gold electrodeposition, Electrochim. Acta 53 (9) (2008) 3449–3458, doi:10.1016/j.electacta.2007.10.037.

[50] A. Stierle, E. Vlieg, Surface-Sensitive X-ray Diffraction Methods, John Wiley & Sons, Ltd, 2012, pp. 221–257, doi:10.1002/9783527649884.ch8.

[51] L.-M. Peng, G. Ren, S.L. Dudarev, M.J. Whelan, Debye waller factors and absorptive scattering factors of elemental crystals, Acta Crystallogr. Sect. A FoundationsCrystallogr. 52 (3) (1996) 456–470, doi:10.1107/S010876739600089X.

[52] M.J. Rost, L. Jacobse, M.T. Koper, Non-random island nucleation in the electrochemical roughnening on Pt(111), (2021), to be submitted.

[53] Z. Duan, G. Henkelman, Atomic-scale mechanisms of electrochemical Pt dissolution, ACS Catal. 11 (2021) 14439–14447, doi:10.1021/acscatal.1c02366.

[54] N. Seriani, W. Pompe, L.C. Ciacchi, Catalytic oxidation activity of Pt3O4 surfaces and thin films, J. Phys. Chem. B 110 (30) (2006) 14860–14869, doi:10.1021/jp063281r.

[55] D. Fantauzzi, S. Krick Calderón, J.E. Mueller, M. Grabau, C. Papp, H.P. Steinrück, T.P. Senftle, A.C. van Duin, T. Jacob, Growth of stable surface oxides on Pt(111) at near-ambient pressures, Angew. Chemie - Int. Ed. 56 (10) (2017) 2594–2598, doi:10.1002/anie.201609317.

[56] H. You, Z. Nagy, D. Zurawski, R. Chiarello, Place-exchange mechanism of Pt(111) oxidation-reduction as observed by synchrotron X-ray scattering, in: Proc. Sixth Int. Symp. Electrode Process., The Electrochemical Society, 1996, pp. 136–149.